Interaction of Carbon nanoparticles with lipid bilayers

M.Sc. Thesis

by

Kavana M
1803131009

DISCIPLINE OF CHEMISTRY
INDIAN INSTITUTE OF TECHNOLOGY INDORE
JUNE 2020

Interaction of Carbon nanoparticles with lipid bilayers

A THESIS

Submitted in partial fulfillment of the
requirements for the award of the degree
of
Master of Science

by
Kavana M

DISCIPLINE OF CHEMISTRY
INDIAN INSTITUTE OF TECHNOLOGY INDORE
JUNE 2020

INDIAN INSTITUTE OF TECHNOLOGY INDORE

CANDIDATE'S DECLARATION

I hereby certify that the work which is being presented in the thesis entitled **Interaction of Carbon nanoparticles with lipid bilayers** in the partial fulfillment of the requirements for the award of the degree of **MASTER OF SCIENCE** and submitted in the **DISCIPLINE OF CHEMISTRY, Indian Institute of Technology Indore**, is an authentic record of my own work carried out during the time period from July 2019 to June 2020 under the supervision of Dr. Anjan Chakraborty, Associate Professor, IIT Indore.

The matter presented in this thesis has not been submitted by me for the award of any other degree of this or any other institute.

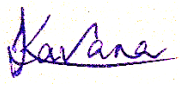

Kavana M

This is to certify that the above statement made by the candidate is correct to the best of my/our knowledge.

Dr. Anjan Chakraborty

Kavana M has successfully given her M.Sc. Oral Examination held on **24th June 2020**.

Signature of Supervisor of MSc thesis

Convener, DPGC

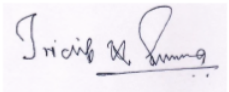

Signature of PSPC Member

Signature of PSPC Member

ACKNOWLEDGMENTS

I would like to give my deepest gratitude to my supervisor, **Dr. Anjan Chakraborty**, for his continuous guidance and support during this project work. He has assisted throughout the entirety of my one year masters project with his salient words of advice and by providing assistance and ideas whenever required.

I would also like to thank my PSPC members, Dr. Tridib Kumar Sarma and Dr. Tushar Kanti Mukharjee, for their support.

I am also very much grateful to Ms. Nishu Kanwa for her valuable suggestion and continuous help towards every field of this project. I am also thankful to Mr. Soumya Kanti De for his helping hands and cooperation in this work.

Moreover, I am filled with gratitude to my family and friends for their support.

Finally, I would like to thank Sophisticated Instrumentation Center (SIC), IIT Indore and IIT Indore for providing infrastructure to conduct my research project.

Kavana M

M.Sc. 2nd year

Dedicated to My Family

Abstract

We herein synthesized differently emissive carbon dots (CDs) and studied their interaction with DMPC lipid bilayer membrane. We synthesized the CDs via hydrothermal method using three isomers of Phenylenediamine (PDA). The synthesized oCD, mCD and pCD, from the precursors oPDA, mPDA, pPDA, respectively were of the sizes around 2-6 nm. These CDs were characterized by UV-Visible absorption spectra, FT-IR spectroscopy and Atomic Force Microscopy (AFM). We found that the synthesized CDs were fluorescent in nature and we confirmed this by steady-state and time-resolved fluorescence spectroscopy. These oCD, mCD and pCDs emit yellow, green and red colors, respectively under single-wavelength UV irradiation (λ= 365 nm). Further, we studied the utility of CD as a probe for bilayer dynamics and the efficiency of CDs as fluorescent acceptors. We established a FRET pair between the donor lipid-PRODAN and the acceptor CDs. We observed that the different CDs synthesized from the isomers of PDA interact with lipid membrane in a different manner. The oCDs were observed to interact more efficiently than mCD and pCDs. The spectroscopic and imaging studies reveal that the oCDs are embedded inside the lipid bilayers, whereas mCD and pCDs induce aggregation in the bilayer membrane by being located on the interfacial region. These observations are attributed to the isomeric precursors and their hydration features and further to the different location of the CDs in the bilayer membrane. Therefore, among all the three CDs, oCDs are potential candidates for bioimaging applications.

TABLE OF CONTENTS

LIST OF FIGURES

Figure 15: Confocal, bright field and merged images for blank DMPC bilayers (a-d); DMPC-oCD system (e-h); DMPC-mCD (i-l); and DMPC-pCD (m-p). Scale bars in the images indicate size of 5 μm.

Figure 16: SEM images for the lipid vesicles composed of DMPC (a); DMPC upon interaction with oCD (b); mCD (c); and pCD (d).

LIST OF TABLES

NOMENCLATURE

nm	Nanometer
°C	Degree centigrade
mg	Milligram
mm	Millimetre
cm	Centimetre
mL	Milliliter
µg	Microgram
M	Molar
µM	Micromolar
mM	Millimolar
h	Hours
ps	Picosecond
τ_i	Lifetime of the i^{th} component
χ^2	Reduced chi-square Amplitude of the i^{th} component
a_i	Amplitude of the i^{th} component in a multiexponential decay
D(t)	Normalized Fluorescence Decay

ACRONYMS

CD	CD
PDA	Phenylenediamine
oPDA	o-Phenylenediamine
oCDs	CDs obtained from oPDA
mPDA	m-Phenylenediamine
mCDs	CDs obtained from mPDA
pPDA	p-Phenylenediamine
pCDs	CDs obtained from pPDA
MLV	Multi-Lamellar Vesicle
LUV	Large Unilamellar Vesicle
GUV	Giant Unilamellar Vesicle
SUV	Small Unilamellar Vesicle
DMPC	1,2-dimyristoyl-sn-glycero-3-Phosphocholine
PRODAN	6-Propionyl-2-Dimethylaminonaphthalene
SEM	Scanning Electron Microscopy
TCSPC	Time-Correlated Single Photon Counting
CLSM	Confocal Laser Scanning Microscopy

Chapter 1

Introduction

(1.1) Carbon quantum dots: CDs are a novel class of nanomaterials having sizes less than 10 nm and quasi-spherical morphology [1-2]. CDs comprise of a carbon core having various rich surface-functionalized groups [1-4]. CDs are an emerging area of interest lately considering their diverse applications in nanotechnology, biology, optoelectronics and catalysis due to their excellent photoluminescent properties [2-5]. Owing to the properties such as chemically inert, low toxicity, water solubility, great biocompatibility, good quantum yield, high resistance to photobleaching, and exceptional photoluminescence, CDs have gained superiority over various organic dyes and semiconductor quantum dots [3-10]. Hence, they have wide applications in bioimaging, sensing, bio-labeling, drug delivery, and light emitting diodes [2-10]. Currently, there are two approaches for the synthesis of CDs, namely top-down and bottom-up approaches wherein the former utilizes bulk carbon materials such as graphene or carbon nanotubes, whereas the latter utilizes organic precursors [6,9]. In the Top-down approach, carbon sources are cut into CDs by methods like arc-discharge, electrochemical synthesis, chemical oxidation, or laser ablation [9-11]. The Bottom-up approach involves the preparation of CDs from small organic molecules by various methods assisted by microwave, hydrothermal/solvothermal method, or pyrolysis [9-12].

(1.2) Lipid Bilayers (Liposomes): Cell membranes are mainly composed of phospholipid and membrane proteins [13]. Lipids are composed of two important parts that form the lipid bilayer. The first part is the hydrophilic part which is also known as the polar head group and the other is the hydrophobic part which consists of the long hydrocarbon chain, known as the nonpolar tail [14-15]. A lipid bilayer is formed by the arrangement of lipid molecules when they are injected in polar solvents like water. The polar region in the phosphate group of a lipid bilayer is attracted to water whereas the fatty acid tail is repelled by water

and hence the hydrophilic parts expose themselves to polar solvents whereas the hydophobic parts tend to stay away from water molecules during the lipid bilayer formation as shown in **Figure 1** [13-17]. Liposomes, shown in **Figure 2**, are spherical vesicles consisting of minimum one phospholipid bilayer [13].

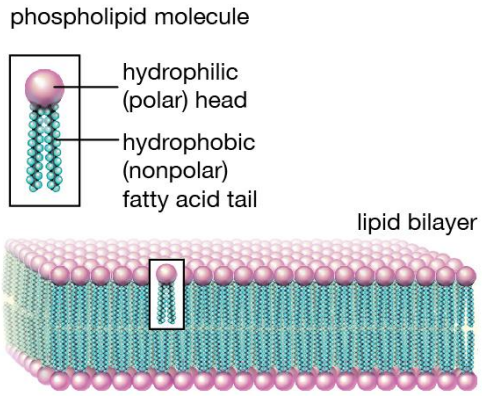

Figure 1: Phospholipid bilayer [17]

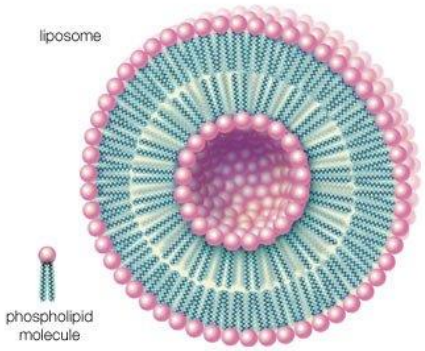

Figure 2: Liposome [17]

Several methods such as thin film hydration [18], solvent injection [19] and reverse phase evaporation [20] are employed for the preparation of lipid bilayers from lipids. Lipid bilayers are classified as Multi-Lamellar Vesicle (MLV), Giant Unilamellar Vesicle (GUV), Large Unilamellar Vesicle (LUV) and Small Unilamellar Vesicle (SUV) on the basis of their sizes, wherein the size of MLV is >0.5µm, GUV is >1µm, LUV is > 100 nm, SUV is 20-100 nm [21-23].

1,2-dimyristoyl-sn-glycero-3- phosphocholine (DMPC) is a zwitterionic lipid molecule that contains phosphate and choline groups. **Figure 3** shows the structure of the two zwitterionic lipids DMPC.

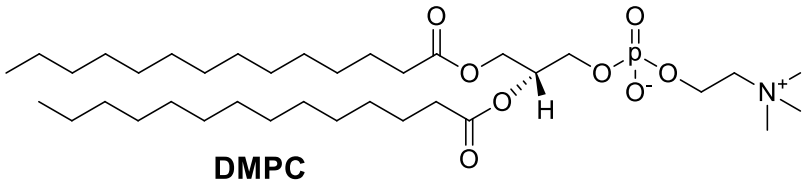

Figure 3: Molecular structure of the lipid DMPC.

In recent past, lipid bilayer membranes have drawn our attention to their interaction with nanoparticles [24-31]. Bilayer fluidity, molecular diffusion in membranes and lipid mobility are the dynamic properties of model membranes which mainly determine the functions of the cell membrane, and modulation of these properties by membrane-active molecules results in cell signaling, biomolecular recognition, drug uptake and several such important cellular processes [32-35].

(1.3) Fluorescent Probes: Fluorescent probes are molecules whose fluorescence emission changes with respect to change in their immediate environment, chemical reaction or a binding event. [36]. Fluorescent probes can yield information about physiological and biochemical properties in biological samples both quantitative and qualitatively, and provide insights on the membrane structure and dynamics, and organization [37-38]. By introducing fluorescent probes in the membrane, membrane heterogeneity i.e. shape and size can be detected and additionally, fluorescent probes can also be utilized to study the local physical properties within the membrane, such as fluidity, polarity, and molecular probe diffusion [39]. Fluorescence molecular probes can be used in this context to study the changes in the dynamics and properties of the bilayer membrane. Thus, membrane polarity sensitive fluorescence probes are taken for this purpose. Earlier, apolar probes such as DPH and pyrene were used, but recently focus diverted to complex amphiphilic probes, e.g., BODIPY, NBD, cyanine dyes or

rhodamine [40]. The emission wavelength and intensity can be monitored by using fluorescence probe. PRODAN (6-Propionyl-2-Dimethylaminonaphthalene) is particularly used in this work among other spectral-sensitive probes because of it's sensitivity to the polarity of the surrounding medium [41]. **Figure 4** shows the structure of the PRODAN. In aqueous media, this probe shows less intensity fluorescence but in membrane medium, they show large intensity fluorescence which is well studied in the literature. When the solvent polarity is increased, a large amount of redshift in the PRODAN emission spectra is noticed due to the dipolar relaxation phenomenon [41-43].

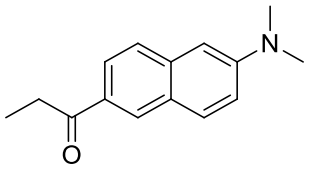

Figure 4: Molecular structure of PRODAN.

(1.4) Forster resonance energy transfer (FRET): Förster resonance energy transfer (FRET) is a non-radiative mechanism of energy transfer from a luminescent donor to an energy acceptor having a lower energy excited state, within a range of around 10 to 100 Å [44–46]. Over the past few decades, even at a single molecule level, FRET based spectroscopic rulers have emerged as a vital tool in studies related to chemical, biological and biochemical processes for the measurement of inter- and intra-molecular distances and mainly for the determination of the conformational biomolecular changes and molecular interactions [47-48]. FRET has emerged as a sensitive and strong approach in monitoring the attachment processes and changes in the dimensionality and configurations of systems [46-50]. Although the origin of the FRET process is dipole-dipole interactions, the energy transfer between the donor and acceptor is highly reliant on distance between their centers [51]. FRET is a powerful approach for studies related to the lipid membrane interactions and dynamics, and especially trans-membrane FRET is a rarely explored process that involves donor and acceptor separated in different bilayer regions [52-53]. FRET has been

broadly employed in fluorescence applications, as well as in medical diagnosis, biological analysis, and optical imaging [54-57]. Recently, numerous research attempts have been made to build CD-based FRET systems as nanoprobes. FRET systems with CDs can be constructed by various fluorescent molecules. Usually, two fluorescent molecules having different emission wavelengths is a requirement for FRET. While constructing a FRET system, the donor CDs transfer energy to another molecule and conversely, the receptors CDs accept energy from other molecules, attaining luminescence via FRET. CD-based FRET systems possess advantages over conventional FRET systems in terms of photobleaching, spectral crosstalk, and direct acceptor excitation. CD-based FRET systems serves as a significant tool as nanoprobes for bioimaging, owing to their good biocompatibility and high sensitivity [58]. FRET efficiency modulation between membrane-embedded donors and acceptors have resulted in changes in bilayer dynamics [59]. Thus, CD-based FRET can be used as a tool for lipid membrane to get insights of the membrane-interactions through various imaging techniques.

(1.5) Studying the interaction of CDs with lipid membrane: Several membrane probes and dyes, have drawbacks such as ineffective insertion into lipid bilayers, disruption of bilayer organization, photobleaching, less fluorescence brightness, and restrictions regarding excitation or emission wavelengths. These limitations can be overcome by CDs since they possess unique photophysical and structural properties [53,60-61]. Especially for biological studies, CDs can be advantageous since they are bio compatible. Furthermore, owing to their low toxicity, chemically stability, low photobleaching and wide-ranging excitation or emission, CDs are advantageous for imaging applications [4-10]. The interaction of CDs and lipid bilayer is an exploring field as they usually give biocompatible results [60-61]. Studies of interaction of CDs with lipid membranes are very few in literature and especially the interaction of differently emissive CDs prepared from isomeric precursors with lipid membrane is not explored so far. Hence, our motive was to study the influence of different fluorescent CDs on lipid membrane by constructing a FRET pair and determine

whether CDs are adaptable and effective candidates for studying bilayer dynamics. We utilized several fluorescence-based biophysical techniques including fluorescence lifetime, and FRET, to analyze membrane bilayer properties. The insertion of CDs into the lipids was studied and applied for analysis and visualization of membrane interactions and bilayer reorganization through imaging applications. This work also reveals that the unique fluorescence properties of the CDs were retained upon interaction and thus, this system can be readily incorporated for bioimaging applications.

Chapter 2

EXPERIMENTAL SECTION

(2.1) Chemicals and Reagents: DMPC (1,2-dimyristoyl-sn-glycero-3-phosphocholine) lipid was purchased from Avanti Polar lipids. The phenylenediamine (PDA) isomer, oPDA was purchased from SDFCL, mPDA was purchased from Alfa Aesar and pPDA from Loba Chemie Pvt. Ltd. All these chemicals were used as received. Milli-Q water was used to prepare all the solutions.

(2.2) Synthesis of CDs: The preparation of CDs was accomplished via hydrothermal synthesis route as shown in **Figure 5**. The precursors oPDA, mPDA and pPDA were dissolved in an ethanol solution (0.1g/mL). This solution was heated in an oven at 180 °C for 12 hours in a hydrothermal autoclave. The CDs were further purified via dialysis. The CDs thus obtained were lyophilized to remove any remaining solvent and the resulting three purified CDs, i.e. oCDs, mCDs and pCDs were dispersed in Milli Q water for further experiments.

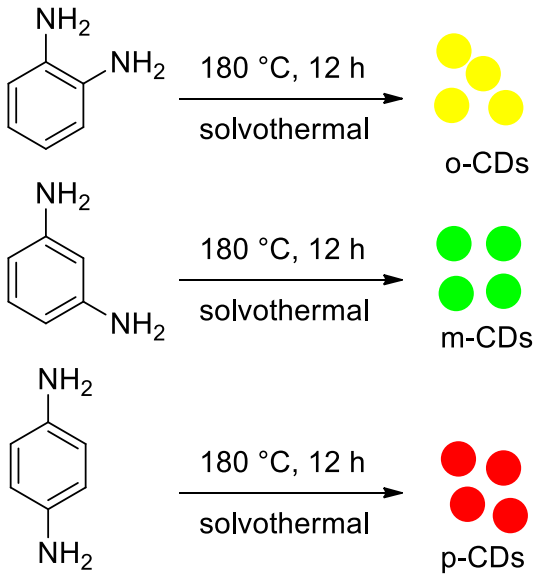

Figure 5: Preparation of yellow, green, red CDs from three isomers of Phenylenediamine (i.e., oPDA, mPDA and pPDA) respectively.

(2.3) Fluorescence spectrum of CDs: To study the fluorescence emission and excitation spectrum of these three CDs we diluted the stock solution to 30 µg/mL. Then we excited all these three CDs according to their respective excitation wavelength and the emission spectrum was recorded. For excitation-dependent spectra, we excited all the CDs in the range of 20 nm starting from their respective excitation wavelength.

(2.4) Preparation of PRODAN solution: A stock solution of 5 mM PRODAN was prepared in ethanol and the required amount of stock solution of PRODAN was taken in a volumetric flask and dried under vacuum for few hours. A required amount of Milli Q water was then added to the volumetric flask to obtain 2 µM PRODAN solution.

(2.5) Preparation of lipid vesicles: Lipid vesicles (0.6 mM) were prepared in Milli Q water. Firstly, PRODAN solution was heated above the phase transition temperature of the particular lipid for 30 minutes. A desired amount of the required lipid was dissolved in ethanol (0.01% of the hydrating solution) and injected in the preheated PRODAN solution. After 90 minutes of stirring the solution, heating was stopped and the solution was allowed to cool for an hour before carrying out further analysis. The lipid concentration was fixed at 0.6 mM and the PRODAN concentration was fixed at 2 µM for all the spectroscopic experiments. The desired concentration of CDs were added to the lipid to perform the titration experiments. Thin film hydration method was employed in the preparation of vesicles for confocal imaging to yield vesicles of ~500-700 nm size. It was later stained with ~20 µM PRODAN dye for atleast 2 hours. Briefly, a thin film of lipid was prepared by dissolving the required lipid in chloroform and it was evaporated using rotary evaporator. The organic solvent was completely removed by storing the obtained thin film under ultra-high vacuum for atleast three hours. This was followed by hydrating the thin film of lipid in aqueous medium above the phase transition of the lipid to obtain MLVs. Thus, uniformly sized lipid vesicles for confocal imaging were obtained by extruding these MLVs.

(2.6) Instrumentation: The absorption spectra of CDs was recorded in Varian UV-vis spectrophotometer (Cary 100 Bio) using a quartz cuvette of size 10 × 10 mm^2. The steady-state fluorescence spectra were recorded in a FluoroMax-4p spectrofluorometer Horiba Jobin Yvon (model: FM100). All the spectra were analyzed using OriginPro 8.1 software. To study the lipid bilayer membrane-CD interaction by varying the concentration of CDs at a fixed concentration of lipid (0.6 mM) and PRODAN (2μM), all the samples were excited at the donor (PRODAN) excitation wavelength i.e. 375 nm. For the titrations, the concentration of the CDs was varied from 2–30 μg/mL. Slit width of 2/2 nm was used for all emission spectra. A temperature of 25 °C was always kept constant throughout all measurements. Picosecond TCSPC machine from Horiba (FluoroCube- 01-NL) was used for lifetime measurements. Here we excited the samples at 375 nm using a picosecond diode laser (model: Pico Brite-375L) and collected decays of the sample at 440 nm. A filter was placed on the emission side to eliminate the scattered light. The signals were collected at a magic angle (54.75°) polarization using a photomultiplier tube (TBX-07C) as the detector. The full width at half-maximum of the instrument response function of our setup was ∼140 ps. The data analysis was performed using IBH DAS version 6 decay analysis software. A fixed the temperature at 25° C was set throughout all titration experiments.

The decays were fitted with a multiexponential function:

$$D(t) = \sum_{i=1}^{n} a_i \exp\left(\frac{-t}{\tau_i}\right)$$

where D(t) represents normalized fluorescence decay and a_i denotes the normalized amplitude of decay component τ_i.

The average lifetime was obtained from the equation:

$$<\tau> = \sum_{i=1}^{n} a_i \tau_i$$

$\chi 2$ values decides the quality of fit and the acceptable fit has a χ^2 near unity.

CLSM imaging was conducted using a confocal microscope from OLYMPUS, model no. IX-83. A Multiline Ar laser (gas laser) with an excitation wavelength of 559 nm was used and the observation mode was laser scanning microscopy (LSM), the scan mode was XY, and the scan direction was one way. The liquid samples were dropped on coverslips and spin-coated before imaging. Thin film hydration method was employed in the preparation of vesicles for imaging, to yield MLVs which were further extruded to get lipid vesicles of uniform sizes. Confocal microscopy was recorded using the laser 405 nm for oCD and mCD and 445 nm for pCD. The emission range was kept 510-610 nm for all the three CDs. Atomic force microscopy (AFM) measurements were performed on a cleaned glass coverslip using NX-10 PARK system. Fourier-transform infrared (FTIR) spectra were recorded using KBr pellets on a Bruker Tensor 27 FTIR spectrophotometer and analyzed using OriginPro 8.1 software.

Chapter 3

RESULTS AND DISCUSSION

(3.1) Characterisation of the synthesized CDs:

Herein, we synthesized three different CDs by using three isomers of Phenylenediamine (PDA) i.e oPDA, mPDA, and pPDA. As mentioned in the experimental section (2.2), the reaction was performed following a bottom-up approach of synthesis via hydrothermal method by dissolving 0.3 g of each precursor in 30 mL ethanol solution separately [12], lyophilized and dispersed in water. The final concentration of oCD, mCD and pCD obtained were 0.57 mg/mL, 0.70 mg/mL and 4.41 mg/mL respectively.

The water dispersion of oCDs, mCDs and pCDs thus obtained show yellow, green and red colors respectively when exposed to UV radiation of wavelength λ= 365 nm, as shown in **Figure 6**.

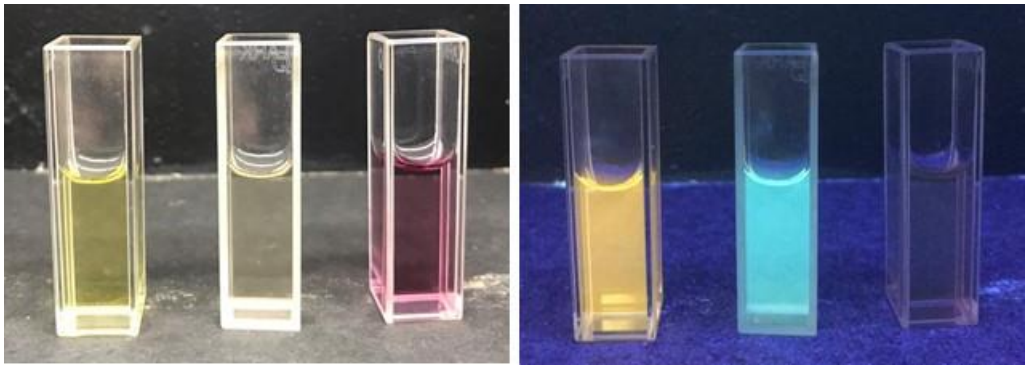

Figure 6: Photographs of oCDs, mCDs and pCDs in visible light (left) and under UV radiation of 365nm (right).

The fluorescence quantum yield of CDs were estimated relative to quinine sulfate (ϕ' = 55% in 0.1 M H_2SO_4) under the excitation wavelength λ_{ex} = 375 nm.

The Quantum Yield of a sample is estimated according to the equation:

$$\phi = \phi' \times \frac{A'}{I'} \times \frac{I}{A} \times \frac{\eta 2}{\eta' 2}$$

where, ϕ is the quantum yield of the CD sample, A′ is the optical density of quinine sulphate, I is the integrated emission intensity of the CD sample, I′ is the integrated emission intensity of quinine sulphate, η is the refractive index (1.33 for water), and A is the optical density of the CD sample.

The quantum yields of oCD, mCD and pCD were calculated to be 10%, 9% and 2.8%, respectively.

FT-IR (Fourier transform infrared) was analyzed to characterize the functional groups and chemical bonds present on these CDs. The three CDs exhibit similar IR spectra as shown in the **Figure 7**, thus revealing the existence of similar chemical compositions. The characteristic peaks around 1225-1234 cm^{-1} can be attributed to the existence of C-O, the peaks around 1336-1384 cm^{-1} confirms the presence of C-N= and the peaks around 2848-2920 cm^{-1} are due to the existence of C-H bonds after the formation of CDs.

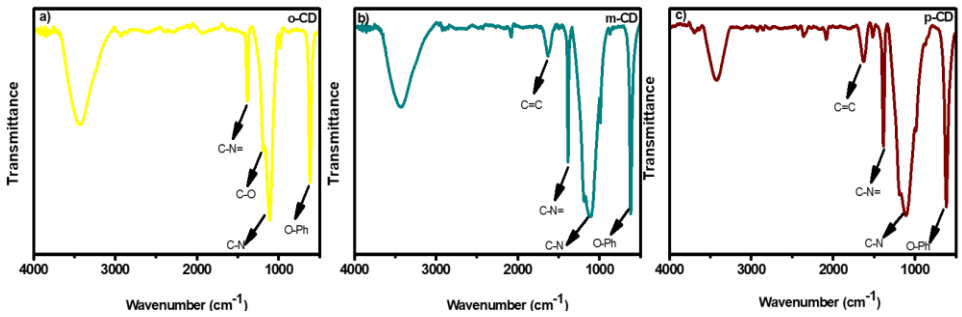

Figure 7: FT-IR spectra of a) oCDs, b) mCDs and c) pCDs.

Further, AFM measurements were performed to find out the morphology and the mean size of the synthesized CDs. The obtained AFM images in **Figure 8** show that all the three CDs are monodispersed and spherical in nature. The size distribution histogram obtained from height profiles reveal the size of oCD to be 4 nm, mCD as 2 nm and pCD as 6 nm. These sizes are in agreement with their respective emission wavelengths.

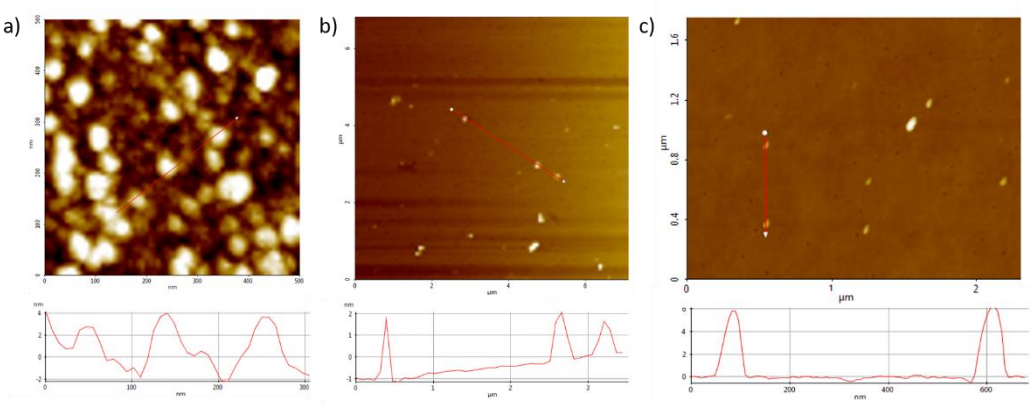

Figure 8: AFM images of a) oCDs, b) mCDs and c) pCDs, bottom: height-profiles analysis along the corresponding lines in figures (a-c).

The UV-Visible absorption peaks of the CDs oCDs was found at 415 nm, mCDs at 375 nm and of pCDs at 435 nm. The emission maxima of oCDs excited at 415 nm was observed at 572 nm. The emission maxima of mCDs excited at 375 nm was observed at 490 nm and similarly, when pCDs excited at 435 nm showed an emission maxima at 635 nm. All these spectra of all the three synthesised CDs were obtained in water solvent and the plots are shown in **Figure 9**.

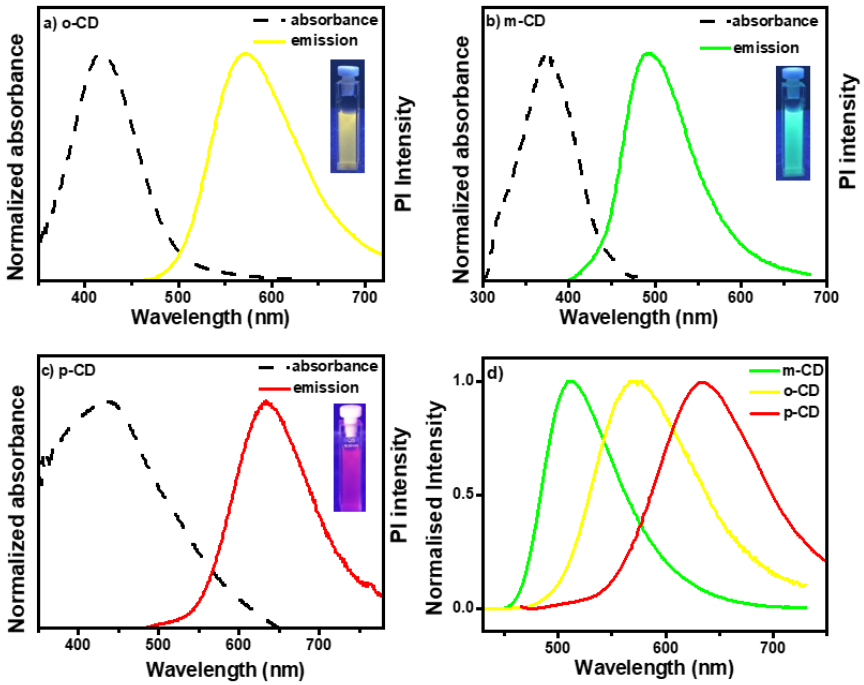

Figure 9: UV/Vis absorption spectra and PL emission spectra of the synthesised CDs a) oCDs, b) mCDs, and c) pCDs, and d) comparison of emission spectra of the synthesized CDs.

A detailed photoluminescence (PL) study was carried out by varying the excitation wavelengths in the range of 20 nm difference for each CD. An excitation-dependent PL spectra of the CDs is depicted in **Figure 10**. The figures reveal that, for different excitation wavelengths, there were slight shifts in emission peak position of the CDs. Therefore, the emission peaks of all the three CDs are excitation wavelength dependent.

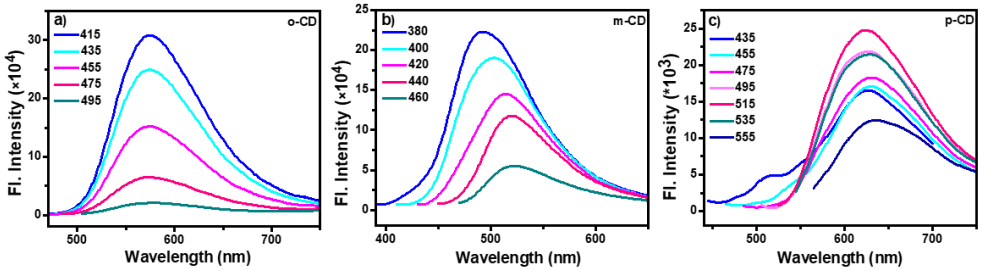

Figure 10: The PL spectra of the synthesized CDs a) oCDs, b) mCDs and c) pCDs upon excitation at different wavelengths.

The time-resolved fluorescence decay curves measured by time-correlated single photon counting method of these CDs are depicted in **Figure 11**. The temperature of 25°C was kept constant throughout the experiments.

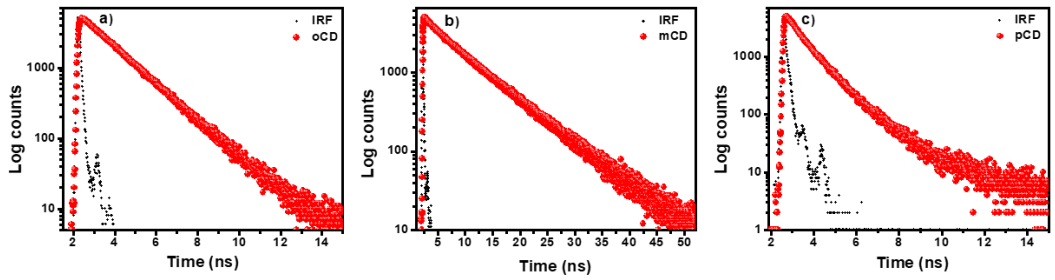

Figure 11: The PL decay spectra of the synthesized CDs a) oCDs, b) mCDs and c) pCDs.

The PL decay of oCD was taken using a laser of 405 nm and the data was collected at 572 nm (emission wavelength). The obtained fluorescence decay

curves of oCD is single-exponential with an average lifetime of 1.63 ns. The PL decay of mCD was obtained using a laser of 375 nm and the data was collected at 500 nm. The lifetime decay curve of mCD was fitted with a bi-exponential function and has a comparitively longer average lifetime of 6.76 ns. The PL decay of pCD was recorded using laser of 445 nm, and the data was collected at 635 nm. The obtained lifetime decay curve of pCD was fitted with a tri-exponential function and has a shorter average lifetime of 0.55 ns (**Table 1**).

Table 1: Time-resolved decay parameters of CDs. Lifetime components, normalized amplitudes of lifetime components and average lifetime of CDs recorded at T = 25 °C.

Sample	**τ_1 (ns)**	**τ_2 (ns)**	**τ_3 (ns)**	**a_1**	**a_2**	**a_3**	**$<\tau_{avg}>$ (ns)**	**χ^2**
	Laser used: 405 nm , Collected at: 572 nm , T=25°C							
oCD	1.63	-	-	1.00	-	-	1.63	1.13
	Laser used: 375 nm , Collected at: 500 nm , T=25°C							
mCD	2.21	7.68	-	0.17	0.83	-	6.76	1.05
	Laser used: 445 nm , Collected at: 635 nm , T=25°C							
pCD	0.67	1.38	0.10	0.39	0.18	0.43	0.55	1.04

(3.2) Studying the interaction of CDs with lipid vesicles:

The interaction of CDs with lipid membrane was studied by comparing the photoluminescene properties of the CDs in aqueous medium vs. in the presence of bilayer membrane. The **Figure 12** shows the interaction of the synthesized CDs with lipid bilayer. The figure illustrates the employment of CDs as a probe for investigating the bilayer dynamics as well as the influence of bilayer environment on the fluorescence properties of the synthesized CDs.

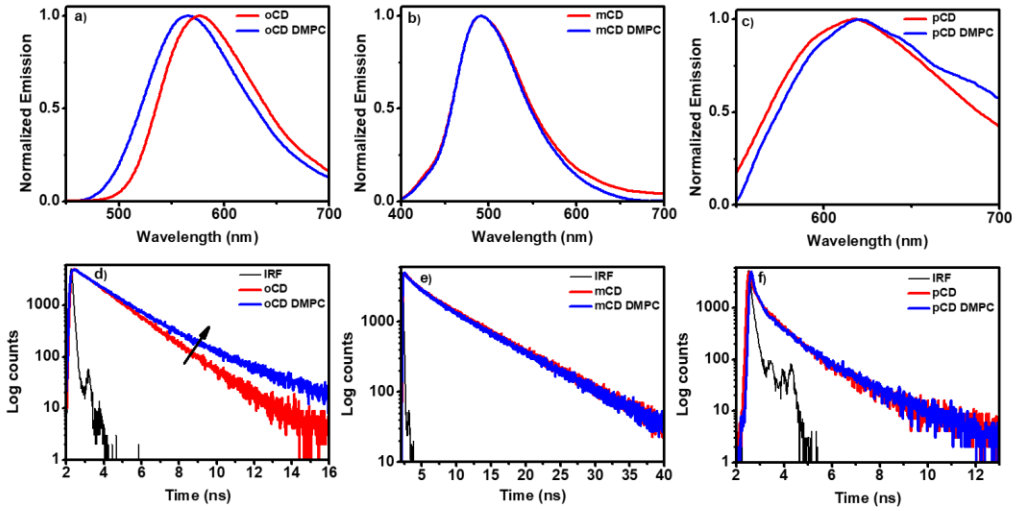

Figure 12: Interaction of the synthesized CDs with DMPC lipid bilayer membrane. Steady state fluorescence spectra (a-c); time-resolved lifetime decay curves (d-f); for a) oCD; b) mCD; and pCD; dispersed in aqueous and DMPC bilayer medium.

Figure 12a reveals that, in case of oCD, there is a significant blue shift in the emission wavelength of oCD from 575 nm (the emission wavelength of oCDs in aqueous medium) to 564 nm upon interaction with DMPC lipid vesicles. The reason behind this peak shift can be attributed to the attachment of oCDs with lipid bilayers. In case of mCD and pCD (**Figure 12b-c**), no such shift in the emission peak is observed and hence we can infer that there is no interaction of DMPC vesicles with mCD and pCD. Additionally, the time-resolved lifetime decays of CDs also reveal their interactions with DMPC bilayer (**Table 2**). The time-resolved lifetime of oCD shown in **Figure 12d**, reveals that the lifetime decay of oCD in aqueous medium is lesser than the lifetime decay of oCD in lipid environment. This confirms it's interaction with DMPC bilayer. Meanwhile, there was no difference in the lifetime decays of mCD and pCD with lipid bilayers as seen in **Figure 12e,f**. Specifically, the decays of oCD was fitted with a single exponential function and oCD DMPC, mCD, and mCD DMPC were best fitted with a bi-exponential function and the decays of pCDs with a tri-exponential function (**Table 2**).

Table 2: Time-resolved decay parameters of CDs in presence of DMPC bilayer membrane. Lifetime components, normalized amplitudes of lifetime components and average lifetime of CDs recorded at T = 25 °C.

Sample	**τ_1 (ns)**	**τ_2 (ns)**	**τ_3 (ns)**	**a_1**	**a_2**	**a_3**	**$<\tau_{avg}>$ (ns)**	**χ^2**
	Laser used: 405 nm , Collected at: 572 nm , T=25°C							
oCD	1.63	-	-	1.00	-	-	1.63	1.13
oCD DMPC	1.50	3.08	-	0.79	0.21	-	1.82	1.16
	Laser used: 375 nm , Collected at: 500 nm , T=25°C							
mCD	1.23	7.56	-	0.36	0.64	-	5.28	1.21
mCD DMPC	1.08	7.53	-	0.32	0.68	-	5.45	1.21
	Laser used: 445 nm , Collected at: 635 nm , T=25°C							
pCD	0.52	1.66	0.03	0.04	0.01	0.95	0.07	1.13
pCD DMPC	0.38	2.00	0.009	0.00	0.00	1.00	0.01	1.10

The lifetime of oCD increases upon interaction with DMPC bilayer as noticeable from **Table 2**, which indicates the insertion of oCDs into DMPC vesicles. In case of the oCDs the average lifetime increases from 1.63 ns in aqueous environment to 1.82 ns in bilayer medium. The appearance of a component around 3.08 ns may be attributed to the CDs inserted in the DMPC vesicles. On the other hand, in **Figure 12**, we notice a negligible change in the average lifetimes and almost no change in the lifetime decay of mCD and pCD on interaction with lipid vesicles, which is in agreement with their fluorescence emission spectra. These results are in agreement with the membrane affinity of the CDs as indicated by the steady state measurements. Thus, it is observed that mCD and pCD do not interact strongly with lipid membrane. These spectroscopic results primarily indicate that lipid membrane displays different affinity towards different CDs. **Figure 12** illustrated the use of CD-DMPC probe for investigating bilayer dynamics. To get further insights of the discriminatory behaviour of lipid bilayers on these CDs, we employed FRET.

(3.3) Employment of CDs as acceptors of energy from lipid-PRODAN as a FRET pair.

The FRET experiments depicted in **Figure 14** indicate the employment of the CD as a probe for studying dynamics of bilayer and the efficiency of CDs as fluorescent acceptors. We tagged the lipid bilayer with PRODAN molecules to investigate the energy transfer. It is well known that PRODAN gets located at the membrane interface and shows widely different emissions in the presence of different media [41]. We established a FRET pair between lipid-PRODAN and CDs with the donor DMPC-PRODAN transferring energy to the acceptor CDs. Hence, the acceptor CDs quenched the fluorescence emission of DMPC-PRODAN. A good overlap of the absorbance of the acceptor and PL emission spectra of the donor is a pre-requisite for FRET.

Figure 13 depicts the spectral overlap between the emission spectra of DMPC-PRODAN vesicles and the excitation spectra of the synthesized CDs, which is a requirement for an effective energy transfer.

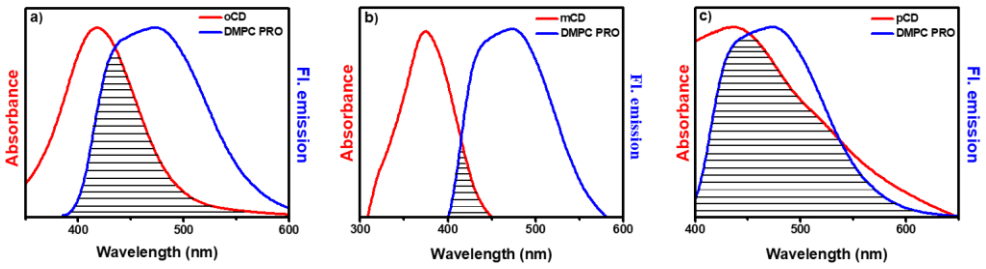

Figure 13: Spectral overlap of the normalized absorbance (red) of the CDs and normalized fluorescence emission spectra (blue) of the DMPC-embedded PRODAN in a) oCD; b) mCD; and c) pCD.

We performed PL measurements shown in **Figure 14a-c** to obtain the relative fluorescene intensity of the DMPC-PRODAN and CD and compared the PL of the combined DMPC-PRODAN-CD system by titration. The final concentration of all the three CDs was kept 30 µg/mL. For an excitation at 375 nm, the fluorescence emission of lipid-PRODAN decreases at around 440 nm in the

presence of the acceptor oCDs, which confirms FRET is a qualitatively. Simultaneously, for oCDs, enhancement in the CD emission maximum PL around 575 nm is observed in **Figure 14a**. This strong increase in the fluorescence indicates the energy transfer from the donor lipid-PRODAN vesicles to the acceptor CDs. In case of mCD and pCDs shown in **Figure 14b-c**, there is no such strong interaction with DMPC-PRODAN as compared to oCDs. Quenching was observed in case of all the three CDs, whereas there was only a little appearance in the emission of mCDs around 520 nm and a negligible increment in case of pCDs around 630 nm as shown in **Figure 14b-c**.

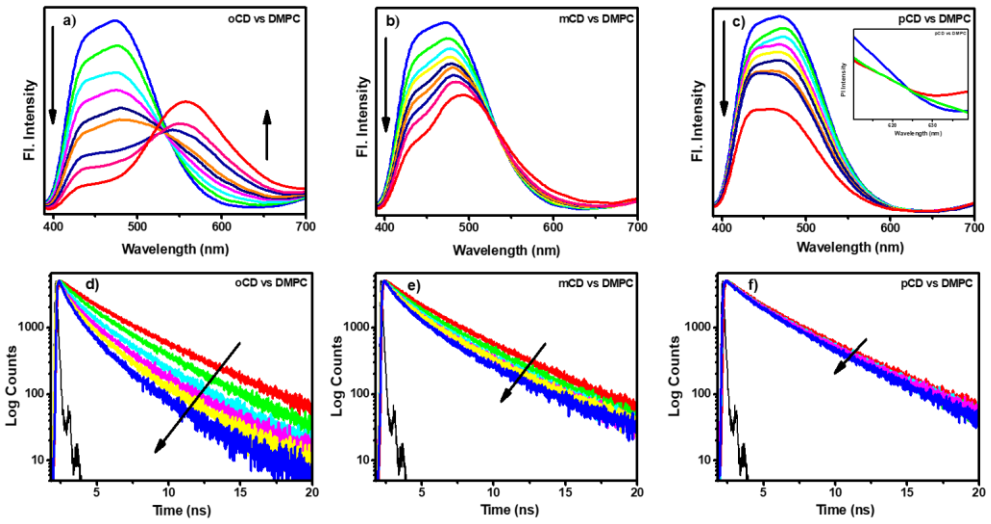

Figure 14: Fluorescence emission spectra of the DMPC-PRODAN upon addition of quencher CDs (a-c); corresponding lifetime decay curves (d-f) in a) oCD; b) mCD; and c) pCD.

We quantitatively estimated the % quenching of DMPC-PRODAN (at 440 nm) upon interaction with different CDs **(Table 4)**, it was found to be 69% for oCD, 56% for mCD and 41% for pCD.

These observations are well supported by time-resolved lifetime decay collected at 440 nm and 25 °C **(Figure 14, Table 3)**, using a 375 nm laser. The observed lifetime fitting data in the **Table 3** reveals a decrease in fluorescence lifetime of the donor in presence of the CDs. Major decrease was observed in the case of

oCD. mCD and pCD had negligible decrease in the fluorescence lifetime of donor. The estimated energy transfer efficiency from the lifetime decay measurements are shown in **Table 4**. The energy transfer efficiency (E) was calculated from the following equation:

$$E = 1 - \frac{\tau_{DA}}{\tau_D}$$

where τ_{DA} and τ_D are the average fluorescence lifetime of the membrane-embedded PRODAN in the presence and in the absence of CDs.

It is observed that a maximum energy transfer takes place for oCD (66%), followed by mCD (40%) and least for pCD (15%). The decrement in the fluorescence lifetime of PRODAN from 3.25 ns to 1.05 ns in the presence of oCD as shown in **Table 3**, clearly indicates FRET. Correspondingly, the quenching percentage estimated from the steady state measurements and the energy transfer efficiency from time-resolved decay data is nearly similar for oCDs (having a quenching percentage around 69% and energy transfer efficiency about 66%). This similarity indicates that energy transfer is the phenomena causing fluorescence quenching of the donor DMPC embedded PRODAN by the acceptor oCD CDs.

Table 3: Time-resolved decay parameters of DMPC-PRODAN in presence of CDs. Lifetime components, normalized amplitudes of lifetime components and average lifetime recorded at T = 25 °C.

Sample (µg/mL)	**τ_1 (ns)**	**τ_2 (ns)**	**τ_3 (ns)**	**a_1**	**a_2**	**a_3**	**$\langle\tau_{avg}\rangle$ (ns)**	**χ^2**
DMPC PRODAN	1.70	4.31	-	0.41	0.59	-	3.25	1.15
oCD 4	1.38	3.81	-	0.50	0.50	-	2.60	1.08
oCD 10	1.09	3.41	-	0.59	0.41	-	2.05	1.22
oCD 15	1.64	0.55	3.74	0.44	0.36	0.20	1.68	1.20

oCD 20	1.42	0.43	3.48	0.46	0.37	0.17	1.40	1.15
oCD 30	1.22	0.33	3.25	0.46	0.42	0.12	1.09	1.25
mCD 4	1.52	4.09	-	0.48	0.52	-	2.81	1.18
mCD 10	1.39	3.95	-	0.54	0.46	-	2.56	1.13
mCD 15	1.28	3.89	-	0.57	0.43	-	2.41	1.15
mCD 20	1.25	3.94	-	0.58	0.42	-	2.37	1.11
mCD 30	1.90	4.71	0.59	0.47	0.18	0.35	1.93	1.22
pCD 4	1.64	4.14	-	0.43	0.57	-	3.09	1.15
pCD 10	1.63	4.22	-	0.43	0.57	-	3.05	1.11
pCD 15	1.58	4.05	-	0.45	0.55	-	2.93	1.13
pCD 20	1.64	4.24	-	0.45	0.55	-	3.06	1.06
pCD 30	1.46	3.91	-	0.48	0.52	-	2.74	1.13

However, the decrement in the fluorescence lifetime of PRODAN for mCD and pCD CDs takes place from 3.25 ns to 1.93 ns and 2.74 ns, respectively. Correspondingly, the estimated steady state fluorescence quenching and energy transfer efficiency in case of mCDs were 56% and 40%, and that of pCDs were 41% and 15%, respectively. Notably, in both the cases, the fluorescence quenching efficiency is much higher than the estimated energy transfer efficiency, revealing that the reason for the fluorescence emission quenching is not just energy transfer.

Table 4: Fluorescence emission quenching percentage and energy transfer efficiency as calculated from time-resolved lifetime for the addition of CDs to DMPC-PRODAN solution.

Acceptor CD	**Fluorescence quenching% (steady state)**	**Energy transfer Efficiency (from time resolved decay)**
oCD	69%	66%
mCD	56%	40%
pCD	41%	15%

According to the above observations, in case of oCD, emission quenching corresponds to the energy transfer, clearly indicating FRET, while for mCD and pCD, the observed results could be because of a non-fluorescent ground state complex formed along with small energy transfer between the membrane-embedded PRODAN and the CDs.

Further, we employed microscopic imaging techniques for studying the effects of CD on the lipid membrane morphology using the photoluminescence properties of these CDs. Confocal images were recorded first at the emission range of PRODAN i.e. 410-480 nm and later at the emission range of CDs around 510-610 nm, to study the interactions clearly. The confocal microscopy images in **Figure 15**, reveal the distribution of CDs inside the bilayers. The images in the **Figure 15e-l** shows the appearance of fluorescent signal of the CDs in the emission range 510-610 nm and depicts that the fluorescent emission signal of the CDs appear from inside the lipid vesicles, remarking the insertion of CDs inside the lipid vesicles. The merged images represent the insertion of CDs inside the lipid vesicles and the corresponding signals. Interestingly, the fluorescence emission characteristics of the CDs were not altered while they were attached to the lipid bilayer, hence we can infer that the fluorescence emission characteristics of the CDs were retained on attachement to the lipid bilayer.

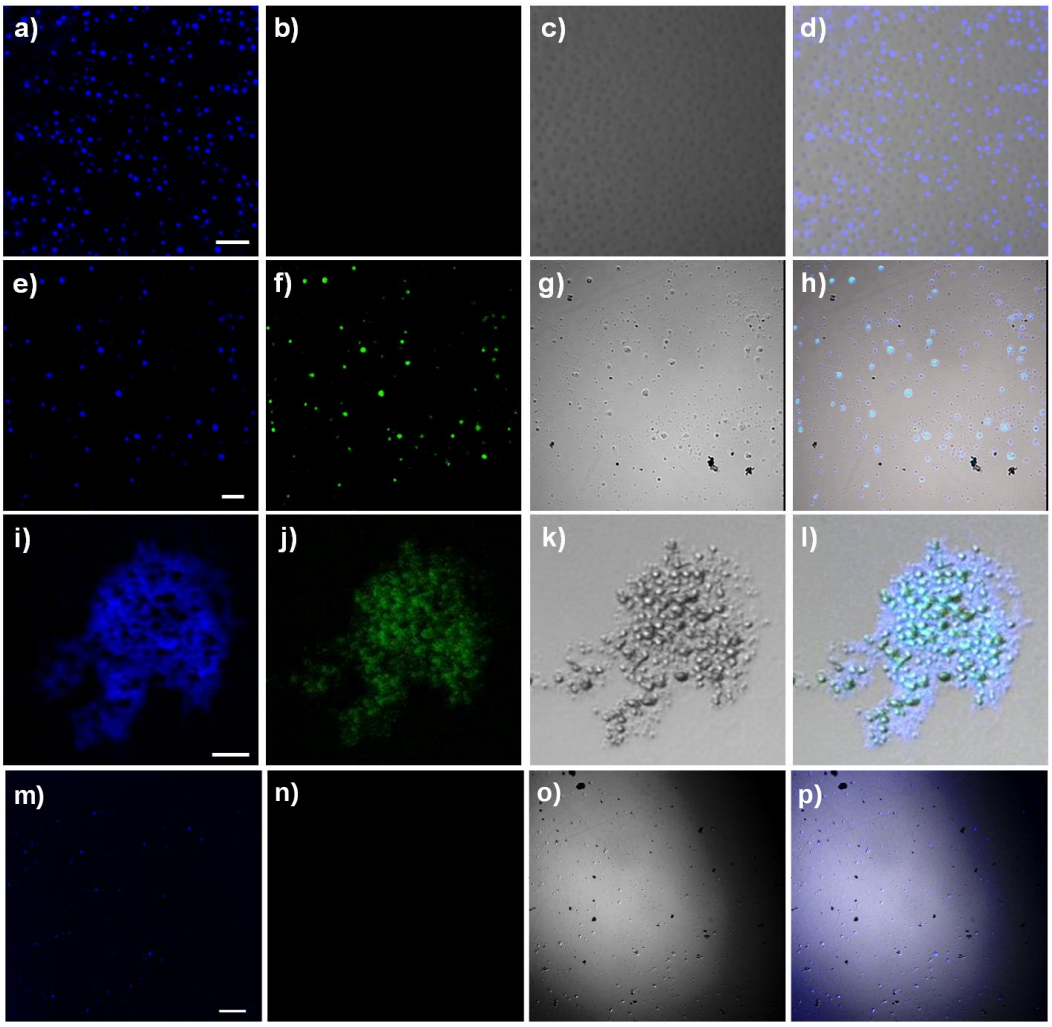

Figure 15: Confocal (emission range 410-480 nm for a, e, i, m and 510-610 for b, f, j, n), bright field and merged images for blank DMPC bilayers (a-d); DMPC-oCD system (e-h); DMPC-mCD (i-l); and DMPC-pCD (m-p). Scale bars in the images indicate size of 5 µm.

In case of oCD as shown in **Figure 15e-h**, we observe that the bilayer membrane maintains it's morphology intact and is not deformed upon interaction. On the other hand, for mCD, shown in **Figure 15i-l**, we observe the aggregation of lipid bilayers upon interaction. No fluorescence signal was observed in pCD upon interaction with lipid membrane as shown in **Figure 15m-p**, owing to the low QY of pCDs. Although from bright field images of pCD in **Figure 15o**, we can infer that the lipid bilayers did not undergo any aggregation. Furthermore, owing to the

excellent luminescence properties and membrane penetrability of the oCDs, we can infer that it can be applicable as a biomarker for cells and model membranes.

Similar observations were demonstrated by SEM images in **Figure 16**. These observations collaborate well with the observations made from confocal microscopy images.

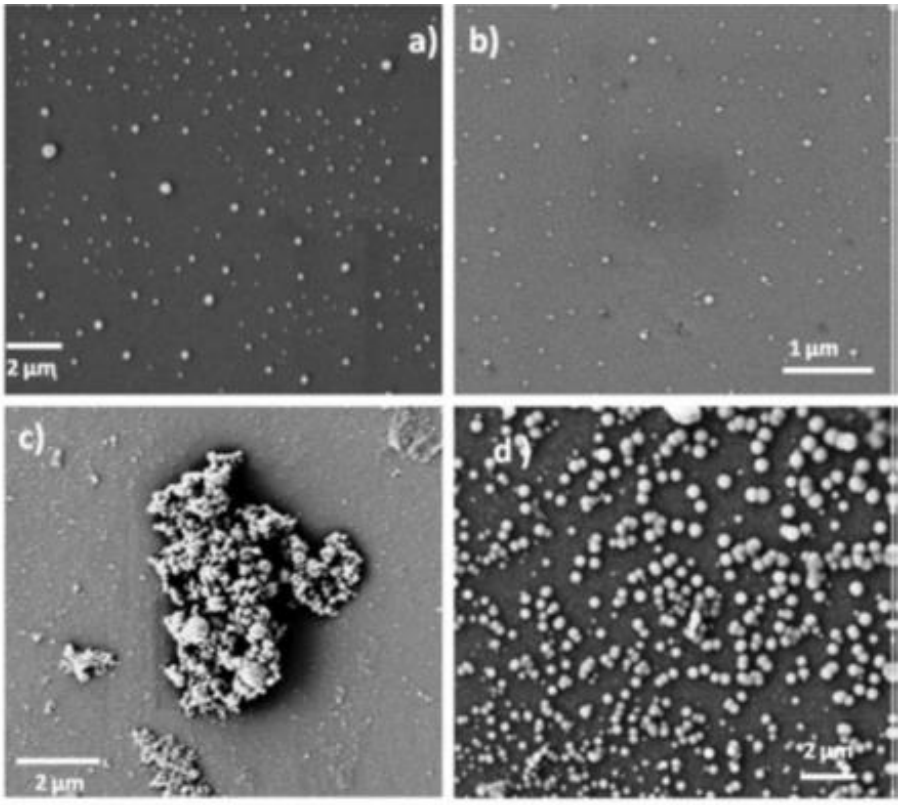

Figure 16: SEM images for the lipid vesicles composed of DMPC (a); DMPC upon interaction with oCD (b); mCD (c); and pCD (d).

It is observed from **Figure 16a** that the lipid vesicles maintain their morphology intact upon interaction with oCD. The interaction with mCD results in total aggregation of the lipid vesicles. Moreover, the sizes of the vesicles increased from their initial structres having 100-200 nm upto few microns as shown in **Figure 16c**. In case of pCD, we notice that the lipid vesicles are comparatively closer to each other, leading to minor aggregation shown in **Figure 16d**.

After all these studies and observations, a question arises about the difference in the behaviour of lipid membrane towards the CDs synthesized from different isomeric precursors. These observations can be ascribed to structural differences of the CD precursors, the o-, m- or p- substitution of the isomeric groups lying at the surface of the CDs, causing self-surface passivation of the CDs [62]. The properties of these CDs are highly influenced by the molecular structures of their precursors. Also, the pKb value of the ortho isomeric precursor, i.e. oPDA, is 9.53 and is the largest when compared to that of mPDA (9.12) and pPDA (7.92). Our results are consistent with a report by L. Song *et al.* that, as the molecular structures of PDA isomers have a considerable effect on the fluorescence properties of the obtained CDs, the fluorescent properties of CDs obtained from m- and p- PDA are completely different from the o- isomer [10]. We observed that oCD CDs gets inserted and penetrate deep inside the membrane. This observation can be attributed to the intramolecular hydrogen bonding among the two amino groups of the o-Phenylenediamine molecule, that lowers the availability of the nitrogen atoms of the amino group to form any further bonding with the head group of the lipids, and due to the environment inside the membrane being less polar, this intramolecular hydrogen bonding is further facilitated. On the contrary, for m- and p- isomers of PDA, the electrons are easily available and may be responsible for the complex formation after interacting at the interface of lipid membrane, leading to static quenching [63]. Now, the question that arises according to our prediction that the mCD and pCD CDs are bound to the head region at the interface of the lipid membrane is, whether there is any change in the lipid membrane morphology due to the interaction? The hydration levels of the different isomeric precursors of the CDs explains this doubt. It is well reported that the hydration features of o- and p- isomers of PDA are totally different from that of m-PDA [64]. For all the PDA isomers, especially near the hydrogen atoms of the amine and the lone-pairs of the nitrogen atoms, the coordinated water molecules get localised, although for m-PDA, to some extent the solvent gets localized to aromatic ring which is the most hydrophobic region, unique from the observations made in case of o- and p- isomers.

Therefore, we propose that during the interaction of mCD with lipid membrane, we observe the overall aggregation of lipid vesicles structure formed as the result of distortion in the structure of spherical vesicles due to the attempt of the solvent molecules trying to propogate to the hydrophobic region of the lipid bound CD. One interesting factor is that the CDs retain their fluorescence properties intact and do not get aggregated themselves during the formation of the aggregated lipid vesicles due to the interaction.

Conclusion

In summary, we synthesized differently emissive CDs and studied the interaction of these CDs with lipid bilayers using a fluorescent probe PRODAN. From the above studies, we summarized the following important observations:

(1) CDs synthesized from different isomeric precursors could be significantly different from each other in terms of their interaction with lipid membrane.
(2) The synthesized oCDs interact strongly with lipid membrane.
(3) According to the spectroscopic studies, oCDs tend to penetrate deep inside the lipid bilayer membrane while the mCD and pCDs remain bound to the interfacial region and induce instability in the membrane and results in aggregation.
(4) Intra and intermolecular hydrogen bonding of the corresponding precursors explains the discriminatory behaviour of lipid membrane.
(5) In conclusion, among all these CDs, only oCD can be favoured as a potential candidate for bioimaging purpose.

REFERENCES

[1] Kwon W., Do S., Rhee S.W. (2012), Formation of highly luminescent nearly monodisperse carbon quantum dots *via* emulsion-templated carbonization of carbohydrates, RSC Adv., 2, 11223.

[2] Baker S. N., Baker G. A. (2010), Luminescent Carbon Nanodots: Emergent Nanolights. Angew. Chem. Int. Ed., 49, 6726.

[3] Huang H., Xu Y., Tang C. J., Chen J. R., Wang A. J., Feng J. J. (2014), Facile and Green Synthesis of Photoluminescent Carbon Nanoparticles for Cellular Imaging, New J. Chem., 38, 784−789.

[4] Sciortino A., Cannizzo A., Messina F. (2018), Carbon Nanodots: A Review—From the Current Understanding of the Fundamental Photophysics to the Full Control of the Optical Response, C — Journal of Carbon Research, 4, 1-35.

[5] Shen J. H., Zhu Y. H., Yang X. L., Li C. Z. (2012), Graphene quantum dots: emergent nanolights for bioimaging, sensors, catalysis and photovoltaic devices, Chem. Commun., 48, 3686.

[6] Liu M. L., Chen B. B., Li C. M., Huang C. Z. (2019), Carbon dots: synthesis, formation mechanism, fluorescence origin and sensing applications, Green Chem., 21, 449-471.

[7] Semeniuk M., Yi Z., Poursorkhabi V., Tjong J., Jaffer S., Lu Z.-H., Sain M. (2019), Future Perspectives and Review on Organic Carbon Dots in Electronic Applications, ACS Nano, 13, 6, 6224-6255.

[8] Li M., Chen T., Gooding J. J., Liu J. (2019), Review of Carbon and Graphene Quantum Dots for Sensing. ACS Sens., 4, 1732-1748.

[9] Wang X., Feng Y., Dong P., Huang J. (2019), A Mini Review on Carbon Quantum Dots: Preparation, Properties, and Electrocatalytic Application., Frontiers in Chemistry, 7, 1-9.

[10] Song L., Cui Y., Zhang C., Hu Z. and Liu X. (2016), Microwave-assisted facile synthesis of yellow fluorescent carbon dots from o-phenylenediamine for cell imaging and sensitive detection of Fe^{3+} and H_2O_2, RSC Adv., 6, 17704-17712.

[11] Li H., Kang Z., Liu Y., Lee S. T. (2012), Carbon Nanodots: Synthesis, Properties and Applications. J. Mater. Chem., 22, 24230−24253.

[12] Jiang K., Sun S., Zhang L., Lu Y., Wu A., Cai C., Lin H. (2015), Red, Green, and Blue Luminescence by Carbon Dots: Full-Color Emission Tuning and Multicolor Cellular Imaging, Angew. Chem. Int. Ed., 54, 5360 –5363.

[13] Chrai S.S., Murari R., Imran A. (2001), Liposomes: a review, Bio Pharm, 14, 10–14.

[14] Akbarzadeh A., Rezaei-Sadabady R., Davaran, S. *et al*. (2013), Liposome: classification, preparation, and applications, Nanoscale Res. Lett., 8, 102.

[15] Gabizon A., Goren D., Cohen R., Barenholz Y. (1998), Development of liposomal anthracyclines: from basics to clinical applications, J. Control Release, 53, 275–279.

[16] Sahoo S. K., Labhasetwar V. (2003), Nanotech approaches to drug delivery and imaging, Drug Discov Today, 8, 1112-1120.

[17] Allen T. M. (1997), Liposomes. Opportunities in drug delivery, Drugs, 54, 8–14.

[18] Thompson T.E. (2020), Lipid. Publisher Encyclopædia Britannica, https://www.britannica.com/science/lipid.

[19] Bangham A. D., De Gier J., Greville G. D. (1967), Osmotic properties and water permeability of phospholipid liquid crystals, Chemistry and physics of lipids, 1, 225-246.

[20] Deamer D., Bangham A. D. (1976), Large volume liposomes by an ether vaporization method, Biochimica et Biophysica Acta (BBA)-Nucleic Acids and Protein Synthesis, 443, 629-634.

[21] Szoka F., Papahadjopoulos D. (1978), Procedure for preparation of liposomes with large internal aqueous space and high capture by reverse-phase evaporation, Proceedings of the national academy of sciences, 75, 4194-4198.

[22] Hong H., Tamm L. K. (2004), Elastic coupling of integral membrane protein stability to lipid bilayer forces, Proceedings of the National Academy of Sciences, 101, 4065-4070.

[23] Kleinschmidt J. H., Tamm L. K. (2002), Secondary and Tertiary Structure Formation of the β-Barrel Membrane Protein OmpA is Synchronized and Depends on Membrane Thickness, J. Mol. Biol, 324, 319–330.

[24] Al-Jamal W. T., Kostarelos K. (2007), Liposome–nanoparticle hybrids for multimodal diagnostic and therapeutic applications, Nanomedicine, 2, 85-98.

[25] Preiss M. R., Bothun G. D. (2011), Stimuli-responsive liposome-nanoparticle assemblies, Expert opinion on drug delivery, 8, 1025-1040.

[26] Paasonen, et al (2010), Gold-Embedded Photosensitive Liposomes for Drug Delivery: Triggering Mechanism and Intracellular Release. J. Control. Release, 147,136-143.

[27] Liu J., Jiang X., Ashley C., Brinker C. J. (2009), Electrostatically mediated liposome fusion and lipid exchange with a nanoparticle-supported bilayer for control of surface charge, drug containment, and delivery, J. Am. Chem. Soc., 131, 7567-7569.

[28] Tan S., Li X., Guo Y., Zhang Z. (2013), Lipid-enveloped hybrid nanoparticles for drug delivery, Nanoscale, 5, 860-872.

[29] Mornet S., Lambert O., Duguet E., Brisson, A. (2005), The formation of supported lipid bilayers on silica nanoparticles revealed by cryoelectron microscopy, Nano letters, 5, 281-285.

[30] Gao W., Hu C. M. J., Fang R. H., Zhang L. (2013), Liposome-like nanostructures for drug delivery, J. Mater. Chem. B, 1, 6569-6585.

[31] Tan S., Li X., Guo Y., Zhang Z. (2013), Lipid-enveloped hybrid nanoparticles for drug delivery, Nanoscale, 5, 860-872.

[32] Pucadyil T. J., Mukherjee S., and Chattopadhyay A. (2007), Organization and dynamics of NBD-labeled lipids in membranes analyzed by fluorescence recovery after photobleaching, J. Phys. Chem. B, 111, 1975–1983.

[33] Guo L., Har J. Y., Wohland T. (2008), Molecular diffusion measurement in lipid bilayers over wide concentration ranges: a comparative study, ChemPhysChem, 9, 721–728.

[34] Tero R. (2012), Substrate effects on the formation process, structure and physicochemical properties of supported lipid bilayers. Materials (Basel), 5, 2658.

[35] Singer, S. J., G. L. Nicolson. (1972), The fluid mosaic model of the structure of cell membranes, Science, 175, 720–731.

[36] Lee M. H., Kim J. S., Sessler J. L. (2015). Small molecule-based ratiometric fluorescence probes for cations, anions, and biomolecules, Chem. Soc. Rev., 44, 4185–4191.

[37] Shorte S. L., Bolsover S. (1999), Fluorescent and Luminescent Probes for Biological Activity, second ed. Elsevier BV, pp. 94–107.

[38] Bouvrais H, Pott T, Bagatolli LA, Ipsen JH, Méléard P. (2010), Impact of membrane-anchored fluorescent probes on the mechanical properties of lipid bilayers**,** Biochim. Biophys. Acta, 1798, 1333–1337.

[39] Jensen E. C. (2012), Use of fluorescent probes: their effect on cell biology and limitations, Anat. Rec., 295, 2031–2036.

[40] Drummen G.P.C. (2012), Fluorescent Probes and Fluorescence (Microscopy) Techniques — Illuminating Biological and Biomedical Research, Molecules, 17, 14067-14090.

[41] Parasassi T., Krasnowska E. K., Bagatolli L., Gratton E. (1998), Laurdan and Prodan as polarity-sensitive fluorescent membrane probes, Journal of fluorescence, 8, 365-373.

[42] Krasnowska E. K., Gratton E., Parasassi T. (1998), Prodan as a membrane surface fluorescence probe: partitioning between water and phospholipid phases, Biophysical journal, 74, 1984-1993.

[43] Wilson-Ashworth H. A., Bahm Q., Erickson J., Shinkle A., Vu M. P., Woodbury D., Bell, J. D. (2006), Differential detection of phospholipid fluidity, order, and spacing by fluorescence spectroscopy of bis-pyrene, prodan, nystatin, and merocyanine 540, Biophysical journal, 91, 4091-4101.

[44] Aron A. T., Loehr M. O., Bogena J., Chang. J. (2016), An Endoperoxide Reactivity-Based FRET Probe for Ratiometric Fluorescence Imaging of Labile Iron Pools in Living Cells, J. Am. Chem. Soc., 138, 14338–14346.

[45] Vafabakhsh R., Levitz J., Isacoff E. Y. (2015), Conformational Dynamics of a Class C G-protein-coupled Receptor, Nature, 524, 497.

[46] Guo J., Qiu X., Mingoes C., Deschamps J. R., Susumu K., Medintz I. L. and Hildebrandt N. (2019), Conformational Details of Quantum Dot-DNA Resolved by Förster Resonance Energy Transfer Lifetime Nanoruler, ACS Nano, 13, 505–514.

[47] Hohng S., Lee S., Lee J., Jo M. H. (2014), Maximizing information content of single-molecule FRET experiments: multi-color FRET and FRET combined with force or torque, Chem. Soc. Rev., 43, 1007.

[48] Schuler B., Lipman E. A., Steinbach P. J., Kumke M. and Eaton W. A. (2005), Polyproline and the “spectroscopic ruler” revisited with single-molecule fluorescence, Proc. Natl. Acad. Sci. U. S. A, 102, 2754.

[49] Thomas III S. W., Joly G. D. and Swager T. M. (2007), Chemical Sensors Based on Amplifying Fluorescent Conjugated Polymers, Chem. Rev., 107, 1339.

[50] Jameson D. M., Ross J. A. (2010), Fluorescence Polarization/Anisotropy in Diagnostics and Imaging, Chem. Rev., 110, 2685.

[51] Ray P. C., Fan Z., Crouch R. A., Sinha S. S., Pramanik A. (2014), Nanoscopic optical rulers beyond the FRET distance limit: fundamentals and applications, Chem. Soc. Rev., 43, 6370.

[52] Azzi A. (1975), The application of fluorescent probes in membrane studies, Q. Rev. Biophys., 8, 237−316.

[53] Pritzl S. D., Pschunder F., Ehrat F., Bhattacharyya S., Lohmüller T., Huergo M. A., Feldmann J. (2019), Trans-membrane Fluorescence Enhancement by Carbon Dots: Ionic Interactions and Energy Transfer, Nano Lett., 19, 3886−3891.

[54] Liu J., Lu Y. (2002), FRET Study of a Trifluorophore-Labeled DNAzyme, J. Am. Chem. Soc., 124, 15208–15216.

[55] Galperin E., Verkhusha V. V., Sorkin A. (2004), Three-chromophore FRET Microscopy to Analyze Multiprotein Interactions in Living Cells, Nat. Methods, 1, 209–217.

[56] Basu S., Needham L.-M., Lando D., Taylor E. J. R., Wohlfahrt K. J., Shah D., Boucher W. et al. (2018), FRET-enhanced Photostability Allows Improved Single-Molecule Tracking of Proteins and Protein Complexes in Live Mammalian Cells, Nat. Commun., 9, 2520.

[57] Yang Y., Liu H., Han M., Sun B. and Li J. (2016), Multilayer Microcapsules for FRET Analysis and Two-Photon-Activated Photodynamic Therapy, Angew. Chem., Int. Ed., 55, 13538–13543.

[58] Miao S., Liang K. and Kong B. (2020), Forster resonance energy transfer (FRET) paired carbon dot-based complex nanoprobes: versatile platforms for sensing and imaging applications, Mater. Chem. Front., 4, 128.

[59] Ghatak C., Rao V. G., Pramanik R., Sarkar S., N. Sarkar. (2011), The effect of membrane fluidity on FRET parameters: an energy transfer study inside small unilamellar vesicle, Phys. Chem. Chem. Phys., 13:3711–3720.

[60] Nandi S., Malishev R., Bhunia S. K., Kolusheva S., Jopp J., Jelinek R. (2016), Lipid-Bilayer Dynamics Probed by a Carbon Dot- Phospholipid Conjugate, Biophysical Journal, 110, 2016–2025.

[61] Nandi S., Malishev R., Kootery K. P., Mirsky Y., Kolusheva S., Jelinek R. (2014), Membrane analysis with amphiphilic carbon dots, Chem. Commun., 50, 10299-10302.

[62] Wang J., Cheng C., Huang Y., Zheng B., Yuan H., Bo L., Zheng M.-W., Yang S.-Y., Guo Y., Xiao D. (2014), A facile large-scale microwave synthesis of highly fluorescent carbon dots from benzenediol isomers, J. Mater. Chem. C, 2, 5028-5035.

[63] Liang Z., Kang M., Payne G. F., Wang X., Sun R. (2016), Probing Energy and Electron Transfer Mechanisms in Fluorescence Quenching of Biomass Carbon Quantum Dots, ACS Appl. Mater. Interfaces, 8, 17478−17488.

[64] Cottone G., Noto R., Fornilia S. L. (1998), Interaction of water with the phenylenediamine isomers Ab initio potential evaluation and molecular dynamics simulation, Faraday Trans., 94, 2337-2342.